Geomorphology 511 (2026) 110404

Contents lists available at ScienceDirect

Geomorphology

journal homepage: www.journals.elsevier.com/geomorphology

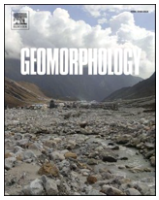

The Apalachicola Barrier Island complex: a benchmark for MIS 5e (125 ka) sea-level oscillations?

Nikos Georgiou [a], Alexander R. Simms [b], Roger C. Creel [c], Silas Dean [a], Denovan Chauveau [d], Ciro Cerrone [a], Claudia Caporizzo [e], Alessio Rovere [a,f,*]

[a] University of Venice Ca' Foscari, Department of Environmental Sciences, Informatics and Statistics, Scientific Campus Via Torino 155, 30172 Mestre, VE, Italy
[b] Department of Earth Science, University of California Santa Barbara, Santa Barbara, CA, 93106, USA
[c] Woods Hole Oceanographic Institution, Woods Hole, MA, 02543-1050, USA
[d] Geo-Ocean, UMR 6538, CNRS, Ifremer, Université de Bretagne Occidentale, F-29280, Plouzané, France
[e] Department of Engineering, Pegaso University, Centro Direzionale Isola F2, 80143, Napoli, Italy
[f] MARUM, Center for Marine Environmental Sciences, University of Bremen, Leobener Str. 8, 28359, Bremen, Germany

A B S T R A C T

The geomorphological and stratigraphic framework of coastal sandy barrier systems preserve records of past sea-level changes, climatic shifts, and storm histories. Recent methodological advances such as Ground Penetrating Radar (GPR), LiDAR topography, and Optically Stimulated Luminescence (OSL) dating now allow for high-resolution reconstructions of these past coastal dynamics, significantly improving our understanding of historical shoreline evolution. Using new GPR and existing LIDAR and OSL ages, we investigate the evolution of the Apalachicola Barrier Island Complex in northwest Florida during the Pleistocene including the Last Interglacial (MIS5e, ~125 ka). Paleogeographic reconstructions show significant barrier morphological changes, including island segmentation and deltaic interactions over multiple highstands including not only MIS5e but potentially older highstands (e.g. MIS7 or older). We find suggestive evidence within the Apalachicola complex for two distinct phases of beach ridge growth linked to early and late MIS 5e sea-level highstands, separated by an erosional unconformity marking a mid-MIS 5e regression and fluvial incision, potentially marking an oscillation in MIS5e sea levels. GPR profiles also record multiple buried storm scarps, indicating major storms approximately every 76 years, assuming similar progradation rates during MIS5e as during the Holocene. Furthermore, the potential oscillation in relative sea level (RSL) at this site in the Gulf of Mexico adds to recent suggestions of a regrowth of the Antarctic Ice Sheet following its putative collapse during early MIS5e.

1. Introduction

Sedimentary coastal systems respond to environmental forcings by retreating, prograding (i.e., advancing horizontally), or accreting (growing vertically) as a response to changes in sea level (Okazaki et al., 2022), storm intensity and direction (Buynevich et al., 2007; Goodwin et al., 2023; Lindhorst and Schutter, 2014), sediment supply, and shoreline evolution (Dougherty, 2018). Prograding sand barriers serve as near-continuous records of paleoenvironmental signals, and studies on their evolution have advanced in the last decades thanks to the development of techniques such as Light Detection and Ranging (LiDAR), Ground Penetrating Radar (GPR), and Optically Stimulated Luminescence (OSL) dating (Fairbridge and Hillaire-Marcel, 1977; Gernant et al., 2025; Rodriguez and Meyer, 2006; Scheffers et al., 2012). These methods allow high-resolution studies of surface and subsurface morphological features and provide chronological constraints on the evolution of sandy barriers.

Prograded sandy coastal barriers are depositional landforms found globally in a range of geological, climatic, and sea-level contexts (Otvos, 2000). They can develop during both rising and falling sea levels (Boyd et al., 1992). Typically, they form in shallow and flat coastal areas with sufficient accommodation and substantial sediment supplies, sourced from either fluvial or long/cross-shore transport (Scheffers et al., 2012). Moderate wave energy is also an important factor in their formation and maintenance. Wave energy needs to be strong enough to move sediment above the mean spring tide level, but not so strong that erosion exceeds deposition. Beyond sediment discharge, wind, storms, and tidal range also govern the beach ridge morphology of prograding sandy coastal barriers (Isla et al., 2023; Tamura, 2012). When sediment accumulation exceeds available accommodation, coastal barriers advance seaward, forming beach ridge systems that preserve near-continuous paleoclimatic and morphodynamic geo-archives (Hein and Ashton, 2020).

* Corresponding author at: University of Venice Ca' Foscari, Department of Environmental Sciences, Informatics and Statistics, Scientific Campus Via Torino 155, 30172, Mestre, VE, Italy.
E-mail address: alessio.rovere@unive.it (A. Rovere).

https://doi.org/10.1016/j.geomorph.2026.110404
Received 27 December 2025; Received in revised form 5 May 2026; Accepted 3 June 2026
Available online 5 June 2026

Under regressive conditions, these systems manifest as sequences of beach ridges and spits, while barrier islands and estuarine strandplains form under transgressive conditions (Isla et al., 2023).

Studies on Holocene beach ridges are widespread (see an overview in Scheffers et al., 2012), but fewer studies have examined Pleistocene beach ridges (e.g., Lopes et al., 2024; Dougherty, 2018; Murray-Wallace, 2018; Oliver et al., 2018), which are generally found landward of their Holocene counterparts. In this paper, we use GPR data from beach ridges along the Apalachicola composite barrier system in Florida (US Gulf Coast) along with high-resolution DEMs and a reanalysis of existing OSL ages to shed light on sea-level oscillations and storm frequency along the Apalachicola beach barrier complex during the Pleistocene including the Last Interglacial (Marine Isotopic Stage, MIS, 5e, 125 ka).

2. Background

2.1. Beach Ridges as archives of past environmental changes

On the horizontal plane (Supplementary Fig. 1), beach ridge systems are represented by shore-parallel to semi-parallel prograding series of ridges and swales (Taylor and Stone, 1996). Their pronounced relief is usually attributed to the development of a foredune ridge of aeolian sand trapped by vegetation on the back barrier. However, lower relief ridges may also form without the presence of an aeolian cap, with the berm's role in shaping this relief still under debate (Hesp, 1984). In the vertical plane (Supplementary Fig. 2), the internal architecture of beach ridges can be examined using GPR surveys. Prograding paleo-beachfaces are expressed as seaward-inclined deposits with inclination varying up to 6° (fine-coarse sand) (Tamura, 2012), being steeper for coarser grains (Jol et al., 1996) and higher wave energy (Hede et al., 2013; Phillips et al., 2019).

Beach ridges are regularly used to reconstruct past sea levels (Gernant et al., 2025; Kumar et al., 2024; Mauz et al., 2013; Montes et al., 2018; Rodriguez and Meyer, 2006; Stattegger et al., 2013). Specific elements within beach ridge systems have been used as Sea Level Index Points (SLIPs), that indicate past sea-level positions in space and time (Shennan, 1986; Shennan et al., 2015). Within beach ridges the facies most commonly used as SLIPs include the Beach-Dune (hereafter referred to as BD) contact, the berm, the Beachface-Upper shoreface contact, and the Upper-Lower shoreface contact (Costas et al., 2016; Rodriguez and Meyer, 2006; Tamura et al., 2007). The BD contact is the uppermost SLIP in a beach ridge and marks the maximum runup of storm waves. On GPR sonograms, the BD is identified as a series of strong, wavy, sub-horizontal, subparallel reflections, with the dipping beachface below showing truncation or toplap structures (Costas et al., 2016). The wave berm, characterized by a flat or landward sloping platform and a slope change at its seaward margin, marks the upper limit of the fairweather swash zone (Costas et al., 2016; Otvos, 2000). Seaward-dipping reflections of the beachface downlapping onto the upper shoreface indicate average low-tide sea levels and are also considered reliable SLIPs as they capture both high and low sea levels and are the last to erode from the foreshore facies (Hede et al., 2013; Nielsen et al., 2017). The erosional contact between the upper and lower shoreface, created by longshore trough migration, can also be a SLIP, though its precision depends on local wave-breaking depth (Hede et al., 2013).

Variations in sediment flux, whether of anthropogenic or climatic origin, directly affect beach ridge frequency and spacing over timescales from months to millennia (Hein and Ashton, 2020; Tamura, 2012). Sediment-starved areas tend to form foredune ridges of higher relief and wider spacing compared to the sediment-rich areas marked by quickly prograding beaches (Carvalho et al., 2019; Nooren et al., 2017; Ruz and Allard, 1994), since sediment starvation leaves dunes more time to accumulate aeolian sand prior to being blocked by a newer dune created during beach progradation. The inverse pattern applies for quickly prograding beach units: higher spatial frequency and lower temporal frequency occurring under conditions of high sediment flux.

Minor variations in wave energy, not including destructive or extreme events, can significantly alter the geometry of the beach face as it alternates between dissipative phases that represent high wave energy events and reflective phases deposited under normal wave conditions (Flemming, 1982; Masselink et al., 2006). Storms cause rapid changes along sandy coasts, affecting prograding beach and dune systems, which preserve geological records of these events, both as depositional and erosional landforms (Goslin and Clemmensen, 2017). Storms can form build-ups (i.e. high beach ridges), which usually consist of coarse-grained material (coarse sand, shells, gravel) and may be the result of single or multiple storm events (Carter, 1986; Butler, 1999). Washover deposits, which contain heavy-minerals, organic content, and shell concentrations, can provide evidence of past storm occurrence and intensity (Goslin and Clemmensen, 2017). They can be recognized by the high energy, landward dipping or horizontal reflectors on GPR profiles of back-barrier sediments, which may form perched fans, sheetwashes, or large scale inlet channels, depending on storm intensity (Carruthers et al., 2013; Donnelly et al., 2006; Masselink and van Heteren, 2014). Even if unconsolidated, large foredunes in prograding beaches prevent storms from breaching barriers, forming erosional scarps by eroding sediments and building bars offshore, which are integrated when the beach is restored back to the reflective profile (Buynevich et al., 2007). These erosional storm scarps are preserved in prograding coasts due to the post-storm recovery infill and, when dated, can record paleo-storm frequency and intensity (Zurbuchen et al., 2020). They are recorded in GPR profiles as high reflectivity, steep seaward dipping strata, and in sediment cores are characterized by heavy minerals (percentage $> 50\%$) and coarse-grained material (Dougherty, 2018; Komar and Wang, 1984).

2.2. The Apalachicola Barrier Island Complex

The "Apalachicola Barrier Island Complex" (Rink and López, 2010) consists of Pleistocene beach ridge deposits landward of a Holocene transgressive barrier chain extending from St Joseph Peninsula to the west to St George barrier island to the east (Burdette et al., 2012, Fig. 1). It is one of the most extensive strandplains in the Gulf of Mexico, with an ~10 km-wide area of discontinuous Pleistocene beach ridges and 6 km of Holocene beach ridges. Sediment is supplied to the strandplain from the Apalachicola River. The Holocene strandplain is shaped by the prevailing Southern swells. A northward prograding spit (St. Joseph Peninsula) and three strandplains prograding towards the south (Cape San Blas, St. Vincent Isl., Little St. George Isl.) constitute the main Holocene coastal barrier system, with the narrow SW-NE extending wave-dominated barrier island of St. George bounding the transgressive Apalachicola Bay to the East (Fig. 1B).

The Apalachicola Barrier Island Complex is the youngest of a series of off-lapping Plio-Pleistocene sandy, presumably marine, sedimentary formations. The northmost separately mapped unit is the Citronelle Formation (*Tci* in Fig. 1A), which consists mainly of quartz sand and gravel, partly deposited as river delta deposits of a late Pliocene-Early Pleistocene nearshore environment (Scott et al., 2001). Seaward of the Citronelle Formation, the Quaternary coastal surface sediments in and around the Apalachicola Delta include Quaternary Holocene sediments (Qh), Quaternary Beach Ridge and Dune (Qbd), Quaternary Alluvium (Qal), and Tertiary/Quaternary Shelly Sediments (TQSu). Otvos (1992) calls the second and fourth of these units the Gulfport and Biloxi Formations, respectively, but they are not formally adopted by Scott et al. (2001) in the most recent Florida Geological Survey map. The Quaternary Holocene Sediments (*Qh*) are mainly marine sands, muds and organic matter (peat) near the present coastline. The Quaternary Beach Ridge and Dune (*Qbd*) sediments are composed of beach ridge belts usually consisting of shoreface to foreshore sand. The Quaternary Alluvium (*Qal*) is Pleistocene and Holocene in age and occurs mainly in floodplains. The Tertiary/Quaternary Shelly Sediments (*TQSu*) include

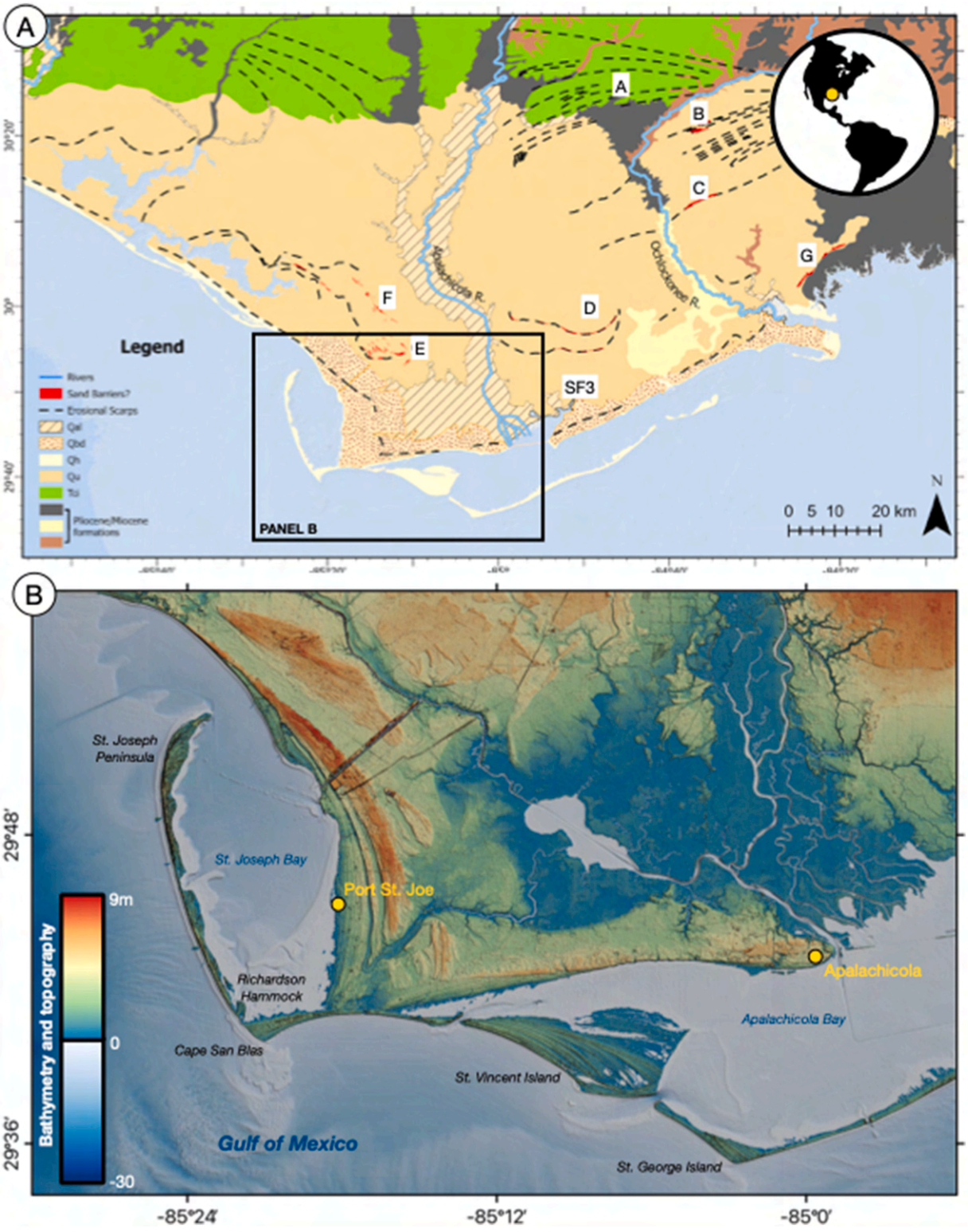

Fig. 1. A) Geologic map of the Apalachicola barrier system (from Scott et al., 2001). Red polygons mark sand barriers; dashed black line marks distinct geomorphological features based on the results of former studies. Labels a-g correspond to locations of geomorphological features shown in Fig. 2. Label SF3 marks the location of the geomorphological feature represented in Supplementary Fig. 3. Legend of geological formations: Qh = Quaternary Holocene Sediments; Qbd = Quaternary Beach Ridge and Dune; Qal = Quaternary Alluvium; Qu = unconsolidated and undifferentiated sediments; Tci = Citronelle Formation. B). Digital elevation model of the study area (NOAA National Centers for Environmental Information, 2023; US Geological Survey, 2011) with toponyms mentioned in the text and main towns.

mainly nearshore fine-grained fossiliferous sediment.

The age of the Quaternary Beach Ridge and Dune (*Qbd*) is controversial: Burdette et al. (2012) use OSL ages retrieved from coastal sediment cores to suggest that the beach ridges formed during the MIS5e highstand. However, deeper sediment cores from the area suggest that the *Qbd* deposits thicken west of the Apalachicola delta, and are composed of two fining upwards sandy Pleistocene sequences, the younger one dated to ~30 ka and the older attributed to MIS5e (Schnable and Goodell, 1968). *Qal* was interpreted as an alluvial cover of MIS6 age overlying the *TQSu*, but Otvos (1992) highlighs inconsistencies in dating and stratigraphic identification of the *Qal* unit. The formation below the *Qbd* and *Qal* (namely, *TQSu*), show an OSL saturated signal (Burdette et al., 2012) suggesting an older age (MIS7/9) than the MIS 5 age proposed by Otvos (1992). To the east of these units, extensive erosion reveals the underlying Miocene-Pliocene formations (Fig. 1A).

Immediately inland of the Holocene coastal barriers, a series of older Pleistocene strandplains is present in the Apalachicola area. The ones closest to the Holocene sequence have been attributed to the Last Interglacial (MIS 5e, 125 ka, Burdette et al., 2012); the existence of deposits dating to previous Interglacials (MIS7,9) or to the MIS6 lowstand in the broader Apalachicola area (*Qu* formation in Fig. 1A) is excluded by Otvos (1992) but supported by Donoghue et al. (1998). The only work providing geochronological ages for Pleistocene coastal sequences in this area is Burdette et al. (2012), who detects a MIS6 alluvium deposit and a fossiliferous nearshore fine-grained formation older than MIS6 (OSL saturated signal) and designates as *TQsu* on geological maps (Scott et al., 2001) and as the Biloxi formation by Otvos (1992), shown as underlying the MIS6 alluvial deposit and the MIS5e beach ridges.

The marine origin of the older and higher Pleistocene terraces and their interpretation as arcuate sand bodies and barrier islands on the unconsolidated and undifferentiated sediments (*Qu* – sand, clay, organics) of the Apalachicola Delta has been contested. Otvos (1995) suggest that these features may be formed by regional tectonic uplift, human activity, e.g. abandoned logging railroad beds and routes or dissolution of underlying carbonates. Conversely, Donoghue et al. (1998) argue for a marine origin of these formations based on sedimentological and geomorphological data (Brenneman and Tanner, 1958; Goetschius, 1971; Stapor Jr et al., 1991) as well as the subsidence of the area (Holdahl and Morrison, 1974). Ionium-disequilibrium dates indicate ages older than MIS5e for these formations (Maxwell, 1971a, 1971b).

3. Methods

To better understand the evolution of the Apalachicola delta, we use the 1/9 arcsecond (~3 m) and 1-m Digital Elevation Models (DEM) from Apalachicola to Pensacola (Fig. 1B, US Geological Survey, 2011, 2022) and a detailed geological map (Scott et al., 2001) to interpret the geomorphology of the Apalachicola Delta Area. We focused on linear structures marking potential former shorelines (dashed black lines in Fig. 1A). In addition to the remote sensing mapping, we visited the more seaward linear structures in the field.

To characterize the subsurface stratigraphy of the most prominent Pleistocene beach barriers in the Apalachicola area and aid in their geomorphic interpretation, we collected 9 km of GPR data using a Sensors and Software EkkoPulse Pro with a 200 MHz antenna. Common-midpoint (CMP) surveys were conducted at each of our six GPR survey sites to determine the velocity of the radar waves within the subsurface. Velocities from these CMP surveys ranged from 0.043 to 0.082 m/ns. GPR profiles were topographically corrected using Global Navigation Satellite System (GNSS) survey data collected at the same time as the GPR. Processing of the GPR lines included automatic gain control and DeWow (a proprietary Sensors and Software processing algorithm). GPR profiles were loaded into EkkoView Deluxe software and ArcMap for interpretation. We assume that the vertical error associated with the identification of a point in the GPR profile is ±0.8 m (1-sigma) based on the variability in radar velocities found throughout the area.

GNSS data were collected with a pair EMLID REACH RS+ receivers (single band) working in Real-Time-Kinematics (RTK) configuration. The position of the base station was initially set to uncorrected coordinates in the field and was corrected in post-processing using the FLCB permanent GNSS station (maintained by the Florida Department of Transportation, located 60-70 km from our study area). All elevation data were referenced to NAVD88 from the GNSS ellipsoid height using the online VDATUM tool by the US National Oceanic and Atmospheric Administration (https://vdatum.noaa.gov/vdatumweb/). Overall, we estimate that the vertical accuracy of this type of positioning is ±0.2 m (1-sigma), including errors due to base postprocessing, rover-base positioning and vertical datum accuracy.

To reconstruct paleo-relative sea level (RSL) from the Beach-Dune (BD) contact identified on GPR profiles, its indicative meaning and associated uncertainty is needed (Shennan, 1986; Shennan et al., 2015). We quantify the BD contact indicative meaning by surveying the modern beach-dune contact in GPR profiles at three locations in the study area (Fig. 3). Two are at Salinas Park on the east side of Cape San Blas (Lines 85 and 86, Fig. 3A); the third is at a public beach access between Lafayette Drive and Martinique Drive on the west side of Cape San Blas (Line 83, Fig. 3A).

4. Results and interpretations

4.1. DEM mapping

Selective fluvial erosion in a SW-NE orientation within the Citronelle Formation formed wedge-shaped channels whose geometry resembles the Holocene progradational landforms throughout the modern Apalachicola Delta. These SW-NE mounds, possibly related to prograding beach deposits, reach maximum elevations of 40 to 56 m (vertical datum: NAVD88, Fig. 2A).

South of these higher and presumably older units, the crests of the curvilinear landforms range in elevation from 30 to 38 m (NAVD88) and are better preserved and of higher relief (Fig. 2B, Fig. 1A) than those in the Citronelle Formation. An erosional scarp, oriented SW-NE at the base of this unit occurs at an elevation of 20 m (NAVD88, Fig. 2C). The same scarp extends to the southwest (Fig. 2C) along the front of a landform interpreted by Donoghue et al. (1998) as a sandbar but whose interpretation is questioned by Otvos (1995). Revisiting these interpretations with higher-resolution DEMs based on LIDAR surveys seems to confirm Donoghue's model as very similar, but better preserved, younger features resembling barriers are observed at lower elevations on both sides of the Apalachicola River (Fig. 2D, E, F). These include seaward concave features (Fig. 2D) resembling delta fronts (Olariu and Bhattacharya, 2006) on the east side of the Apalachicola River with high-relief seaward crests at elevations of 9.5-10 m and 7–7.5 m and wide flat areas (base - Fig. 2D) at 7.5-8 m and 6 m respectively (NAVD88), seaward of the crests. South of these features, cuspate forelands dipping southwards are apparent (Supplementary Fig. 3). On the west side of the river, sandy barrier-like features have crest tops at +6 m average elevation, while the surrounding base lies at +5 m (NAVD88, Fig. 2E). To the NW, these features continue but at increasing elevations, reaching a maximum crest elevations of +9 m and base elevations at +7 m (NAVD88) (Fig. 1A, Fig. 2F), with a characteristic spit-end feature (Fig. 2F inset) at the northeast end. On the eastern side, both sides of the Ochlockonee River have evidence of erosional scarps and spit-barrier features; the features on the river's east side are more prominent (Fig. 2G) and have barrier crests from +8–10.5 m and a scarp carved at +5 m (NAVD88).

Seaward of these ridges and south of the Intracoastal Waterway, are 3 well-defined ridge sets (Fig. 3A). The most landward of these, Beach Ridge Set C, is about 3 km wide and reaches a crest top elevation of 9 m.

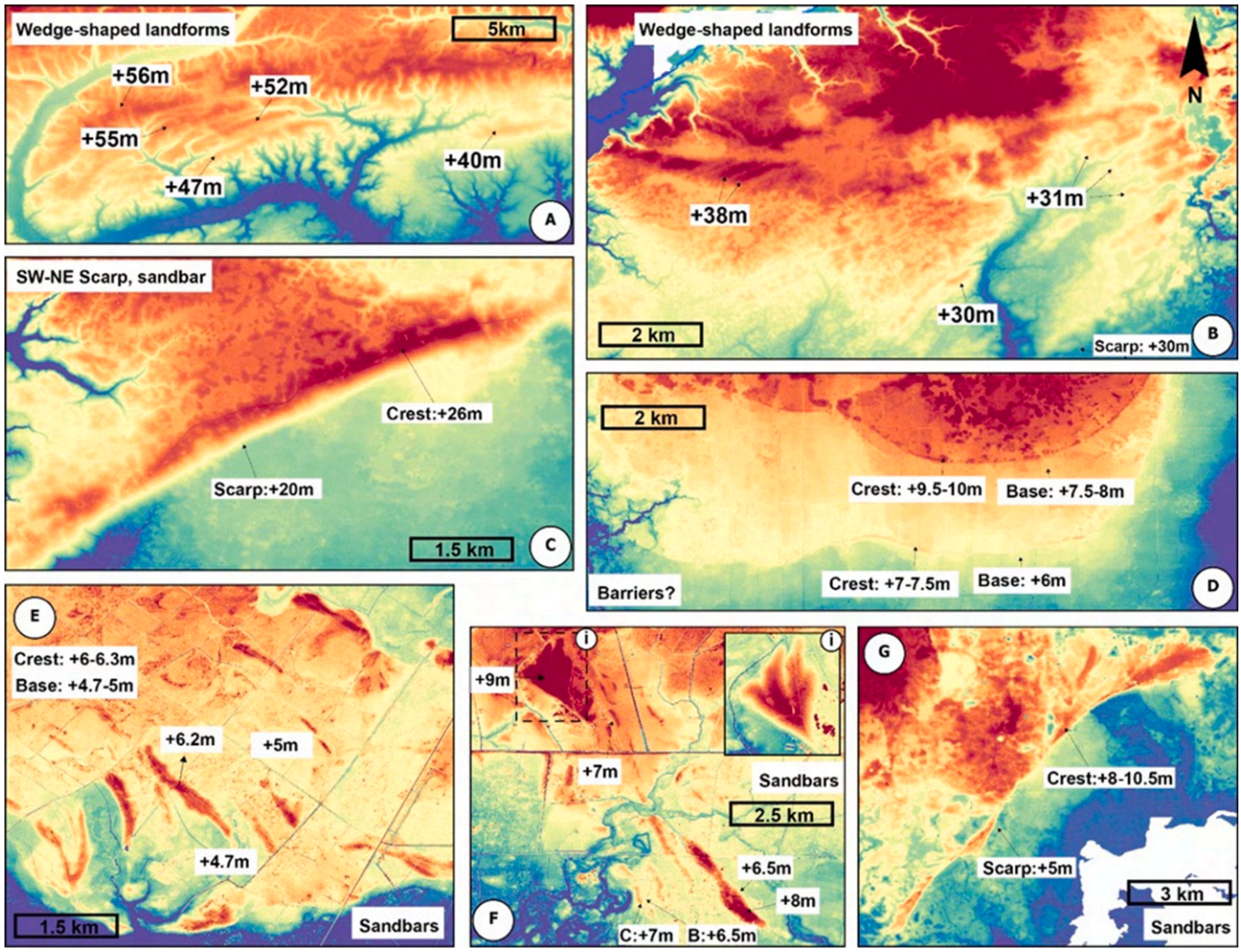

Fig. 2. Distinct geomorphological features related to coastal depositional/erosional features. The location of each panel is shown in Fig. 1A. Elevation data from 1-m DEMs (US Geological Survey, 2022).

Beach Ridge Sets B and A are lower in elevation, ranging from 6 to 8 m and 2-5 m, respectively. They are narrower than Beach Ridge Set C, with average widths of 1.5–2 km. Beach Ridge Set A appears to be a younger continuation of Beach Ridge Set B. Beach Ridge Sets B and A are separated by a trough reaching its lower elevation at 1-2 m above sea level.

4.2. Ground penetrating radar stratigraphy and interpretations

4.2.1. Indicative meaning

Altogether, GPR profiles along the present-day beach (Fig. 4A) indicate that the BD contact is, on average, 0.92 ± 0.46 m (1-sigma) above modern sea level (Fig. 4B). This represents the average and standard deviation of the contact measured in the field, and translates into a reference water level of 0.92 m (indicating that the BD contact forms, on average, 0.92 m above present-day sea level) and an indicative range (i.e., the elevational range occupied by the Bd contact) of 0.92 m (double of the uncertainty range on the BD contact elevation). Therefore, to calculate paleo-RSL from the BD contact measured in Pleistocene deposits, 0.92 m should be subtracted from the elevation of the BD contact. The final uncertainty of paleo-RSL equals the square root of the sum of squares of i) half of the indicative range (0.46 m), ii) GPR vertical error (0.8 m), and iii) GNSS error (0.2 m). By summing these errors using the sum of squares under root mean square formula, the total error associated with paleo-RSL is ±0.94 m (1-sigma).

4.2.2. GPR facies

Three main radar facies were identified in the GPR profiles collected through beach ridge sets A-C and the modern beach. The first radar facies, RF_{sd}, is composed of sets of parallel, seaward dipping reflections. Based on its locations in GPR profiles from the modern beach as well as the generally sandy nature of the deposits underlying this facies, we interpret the RF_{sd} facies to represent foreshore and upper shoreface deposits of a prograding beach/barrier system. The second radar facies, RF_{ld}, is composed of parallel, landward dipping reflections. This radar facies is usually found behind or on the back side of shore-parallel ridges (Line 79, Fig. 5). This radar facies is interpreted to represent washover deposits, possibly into an older lagoon. The third facies, RF_{sbf} is composed of subhorizontal, nearly flatlying reflections. The individual reflections are not as continuous as some of the reflections of the other facies. This radar facies usually unconformably overlies RF_{sd} or RF_{ld} facies. The RF_{shf} is interpreted to represent aeolian dunes overlying older beach foreshore and washover deposits.

Ground-penetrating radar profiles through the RF_{sd} facies towards the end of GPR Line 78 (Supplementary Fig. 4) contain minor erosional discontinuities repeating cyclically for nearly 500 m (Figure). Buynevich et al., 2007 and Zurbuchen et al., 2020 interpreted similar features as erosional surfaces cut by large storms. Given the prevalence of hurricanes and other large storms along the Florida Panhandle, a similar interpretation is taken for these erosional scarps.

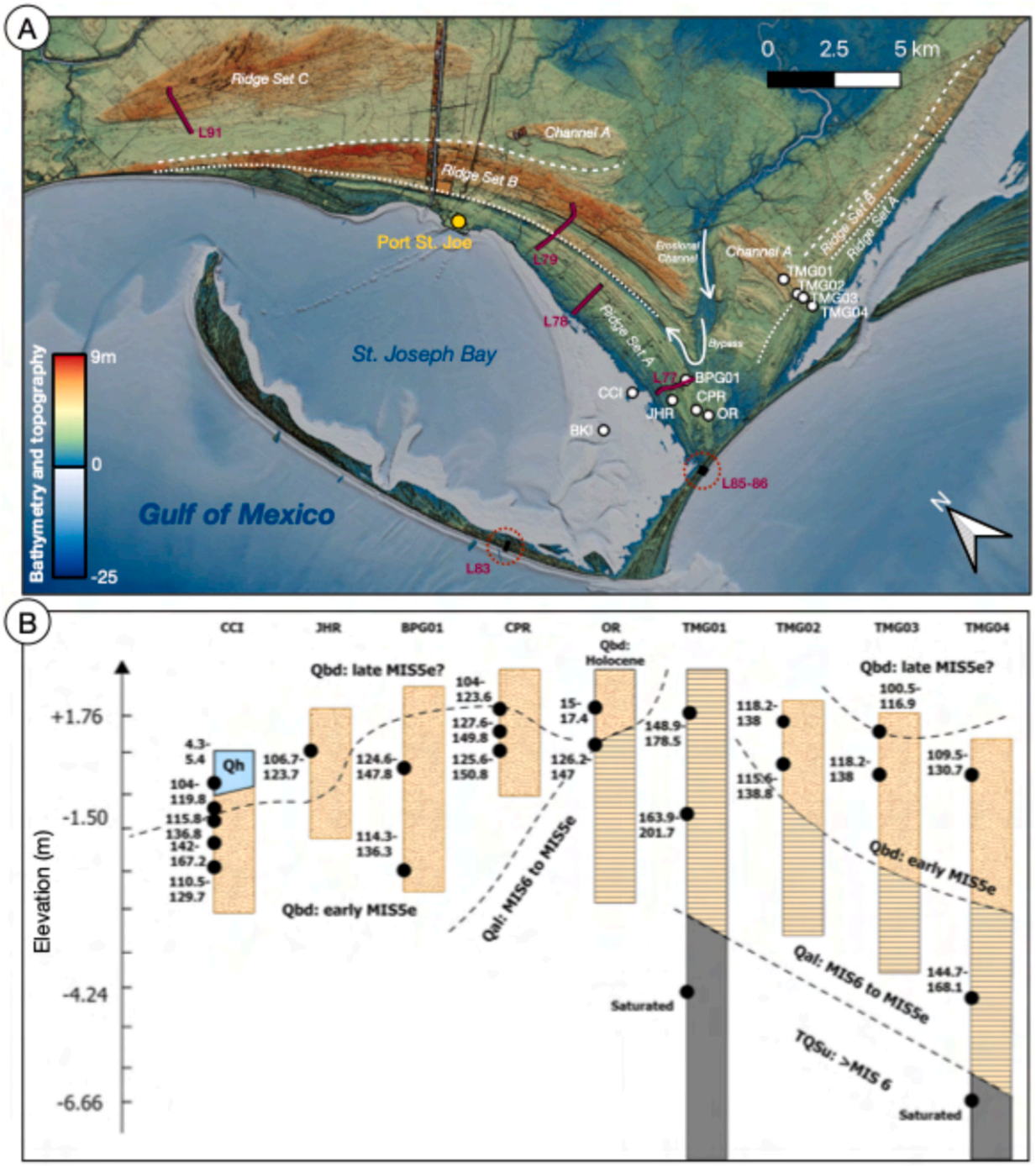

Fig. 3. A) Interpretation of Apalachicola's beach ridge system ages, and correlation with sediment cores from Burdette et al., 2012 (reproduced in Panel B). Elevation data from 1-m DEMs and bathymetry from NOAA (NOAA National Centers for Environmental Information, 2023; US Geological Survey, 2022).

4.2.3. Interpreted beach-dune contact

The contact between RF_{sd} and the overlying RF_{shf} is interpreted to mark the beach-dune (BD) contact (Fig. 5). The elevation of the beach-dune (BD) contact changes through Beach Ridge sets A, B, and C, which were crossed in GPR lines L77, L78 and L79 (Figure). The BD contact crosses both Beach Ridge Sets A and B in GPR line L79 (Figure). Within this GPR line the BD contact drops 4.5 m, from a maximum height of 6.3 m down to 1.8 m (NAVD88). An alluvial infill overlies the seaward dipping beach deposits of RF_{sd} (Fig. 5) while seaward the BD contact rises again, reaching a maximum elevation of 3.9 m. Seaward of this change, the BD contact appears to continuously drop until it reaches the current sea level with a 2 mm per meter of prograding beach (Supplementary Fig. 4).

A major feature interrupting the prograding beach deposits is an alluvial infill whose origin is linked to a sediment bypass feature (Nienhuis et al., 2016) observed at the beginning of L77. Sediment bypass features usually form when waves approach a river mouth obliquely, setting up a longshore current that transports more sediment along the coast than is brought ashore. Based on L78 (Supplementary Fig. 4), the continuity of the beach deposits is interrupted by flat-lying tangent horizons that we interpret as erosional storm scarps (Fig. 6, B-B′ profile). L77 is less clear since it is affected by fluvial and wave erosion as observed on both east and west sides of the profile.

Farther north, within Beach Ridge Set C (Fig. 3A), GPR facies RF_{sd} is

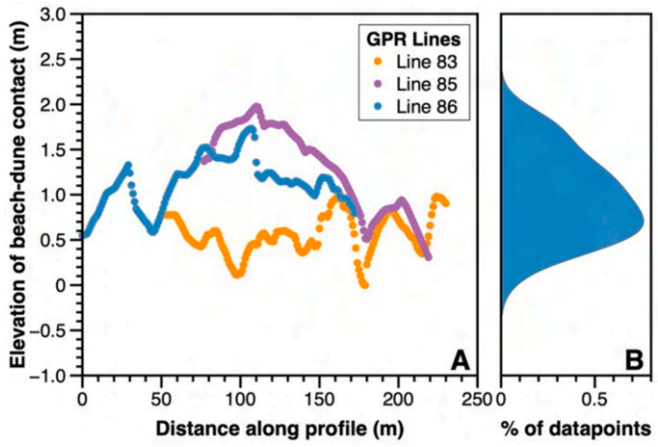

Fig. 4. A) Beach-Dune contact identified along GPR lines across the modern shoreline. B) Density plot of the Beach-Dune contact at the three sites. Elevations are referred to the NAVD88 vertical datum.

also found in GPR line L91 (Supplementary Fig. 6). Within this beach ridge set, the BD contact is found at a nearly constant elevation of 5.9 m for 1 km and gradually decreases seaward to 2.6 m over a distance of 0.9 km (Supplementary Fig. 6). Erosional features interpreted as storm events are also apparent in this unit (Fig. 6, C-C′ profile), similar to GPR-L78 in Beach Ridge Set A. Tracing L91 from south (C) to north (C′), an extended erosional surface interrupts the beach progradation at line distance ~360 m, followed by a zone of hyperbolic reflections, suggesting a different depositional environment (Supplementary Fig. 6).

4.3. Interpreted beach ridge set ages

Giving an age to the beach ridge sets we identified in our work without contextual cores and ages is not straightforward and must rely on correlations with previous literature. The only OSL ages available in this area are those reported by Burdette et al. (2012), who investigated the eastern part of our study area (Fig. 3A), where we did not perform GPR surveys. Beach Ridge Set A (Fig. 3B) surveyed in GPR lines 77, 78, and the seaward-most reaches of 79 onlaps onto Beach Ridge Set B, and a similar architecture as that found in our Beach Ridge Sets A and B is found to the east underlying another transect of OSL-dated cores by Burdette et al. (2012), which point to a MIS 5e age for both ridge sets (Fig. 3B). Therefore, we interpret these two Beach Ridge Sets A and B as distinct periods of beach ridge strandplain progradation. The younger Beach Ridge Set A ranges in elevation from 0 to 4.5 m and we propose that it formed in late MIS5e. MIS 6 deposits were dated by Burdette et al. (2012) below marine/coastal sediments associated with a second, more landward ridge (Fig. 3A). We propose that the older Beach Ridge Set B formed during early MIS 5e. Beach Ridge Set C is located farther inland and ranges in elevation from 4.3 m to 8.5 m. It is disconnected from the two seaward Beach Ridge Sets A and B (Fig. 3A). We suggest that this strandplain, surveyed in GPR line L91 (Figure and Supplementary Fig. 6), is older than the Last Interglacial and may represent the imprint of a former highstand (MIS7, MIS 9 or MIS11).

In the following sections, we discuss our results accepting the hypothesis that Beach Ridge Sets A and B were formed, respectively, during late and early MIS 5e. However, we note that an early MIS 5e age for Beach Ridge Set C, or the attribution of Beach Ridge Sets A and B to distinct interglacials cannot be excluded a priori without radiometric ages.

5. Discussion

5.1. Pleistocene relative sea-level changes

From the descriptions above, GPR profiles L78, L79 and L91 preserved the clearest and most continuous evidence of the BD contact. Applying the indicative meaning of the modern BD contact (Fig. 4) to the elevation of the BD contact along these profiles allows the reconstruction of RSL changes during the late Pleistocene. Overall, the most striking features are the suggested RSL oscillations identified in the GPR profiles.

GPR Line 91 runs through Beach Ridge Set C, interpreted to have formed during an interglacial older than MIS 5e. RSL remains stable for enough time for the beach to prograde 1.0 km before falling to 2.6 m (Figure A). For Beach Ridge Sets A and B, higher sea levels are recorded for Beach Ridge Set B in GPR Line 79 (Figure B), which we correlate to early MIS 5e, than for Beach Ridge Set A, which we correlate to late MIS5e. Starting from a peak RSL of ~5 m, like the initial RSL in GPR Line 91, RSL drops then rises rapidly to 4 m above present (Figure B). Sea level then falls again (Figure B). GPR Line 78 indicates continued sea-level fall through the end of the LIG recorded in our profiles (Figure C).

5.2. Potential RSL implications

Without a precise age assignment for Beach Ridge Sets A and B, it is prudent to remain cautious in speculating about the origins of the MIS-5e RSL oscillation that we propose. Nevertheless, their relative age based on stratigraphic superposition enables us to weigh several possible origins. First, the RSL oscillation could be caused by the isostatic response to sediment loading and unloading of the shelf during phases of increased or decreased sedimentation from the Apalachicola River delta. Sediment isostasy is capable of driving departures from eustasy of several meters between the present interglacial and the LIG (Simms et al., 2013; Pico, 2020), particularly in areas with rapid sedimentation such as the northern Gulf of Mexico. However, magnitudes of land motion calculated for the LIG (Simms et al., 2013) and Holocene (Kuchar et al., 2018) shorelines outside of the Mississippi Delta are too low to fully explain the swings suggested by our GPR data.

Next, we might consider ice sheet melt and glacial isostatic adjustment as origins for the Apalachicola RSL oscillation. Because the Apalachicola Delta sits on the Laurentide Ice Sheet's peripheral bulge, RSL is sensitive to solid Earth effects associated with Laurentide melt as well as the fingerprints of Antarctic and Greenland excess melt. Antarctic Ice Sheet reconstructions during MIS-5e consistently find excess melt of >3 m global mean sea level equivalent prior to 126 ka (Barnett et al., 2023; Golledge et al., 2021; Kopp et al., 2009), a contribution supported by evidence that the West Antarctic Ice Sheet may have collapsed during MIS-5e (Lau et al., 2023) and prior to 126 ka (Wolff et al., 2025), accompanied by substantial East Antarctic melt (Iizuka et al., 2023).

The melting and regrowing of Earth's ice sheets at different times during MIS-5e could have contributed to an oscillation in Apalachicola RSL both through changes in GMSL and through glacial isostatic adjustment (GIA), which describes the viscoelastic response of the solid Earth to changes in ice and water loading (Farrell and Clark, 1976). When out of phase, ice sheet contributions to GMSL can mask each other (Raymo et al., 2006). Thus, whether MIS-5e GMSL oscillated by <1 m (Dyer et al., 2021) or < 4 m (Kopp et al., 2013), much larger fluctuations in individual ice sheets could have occurred so long as the timing of peak melt varied (Creel et al., 2026). And because of the differing sea-level fingerprints of each ice sheet (Hay et al., 2014), these ice sheet asymmetries could have led to rapid fluctuations in Apalachicola sea levels.

Even without GMSL changes, the GIA associated with asymmetric MIS-5e ice sheet melt could have led to a multi-meter oscillation in RSL in the Gulf of Mexico (Creel and Austermann, 2025, Figure D). Creel and Austermann (2025) built an ensemble of ice sheet simulations in which simultaneous early MIS-5e Laurentide persistence and West Antarctic

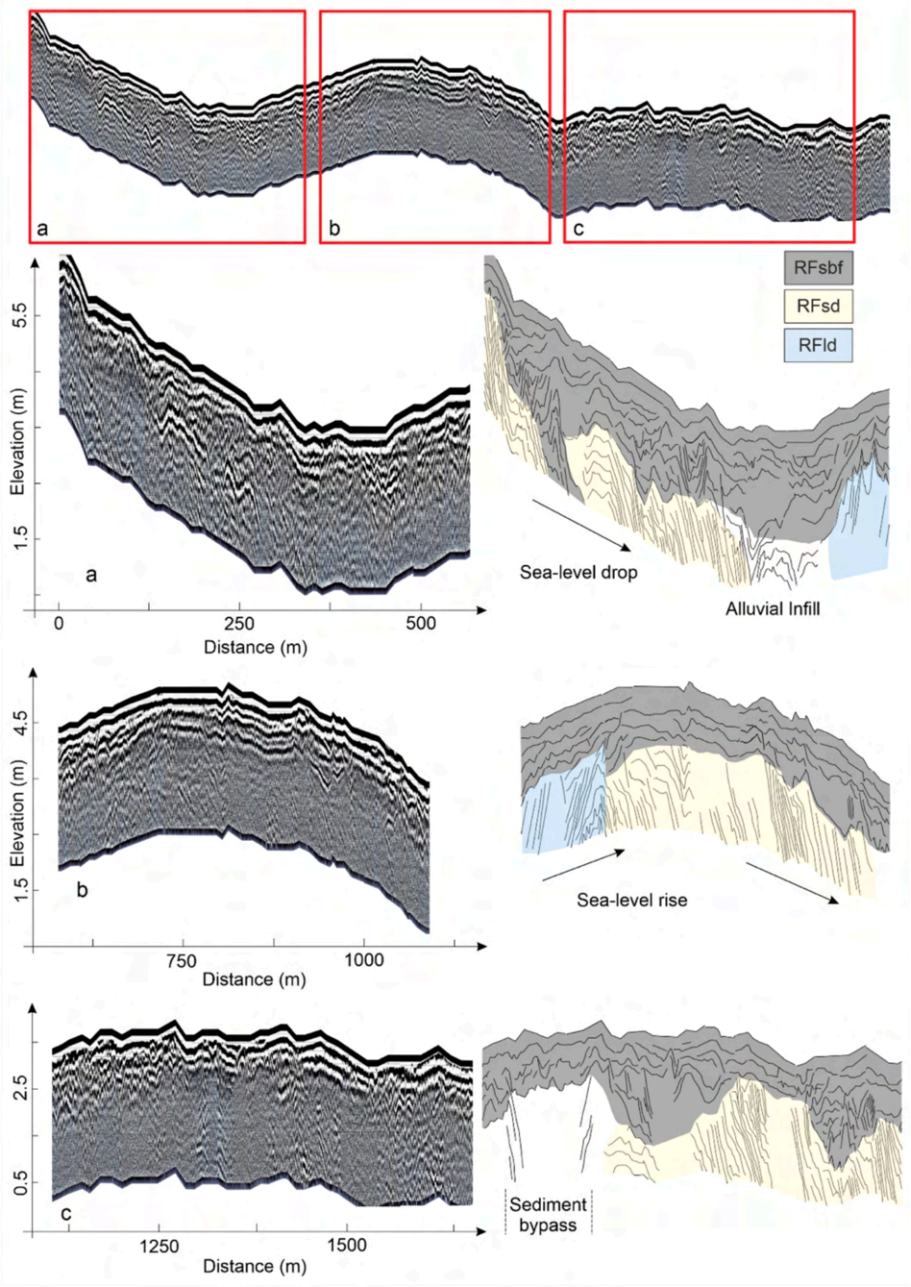

Fig. 5. Interpretation of the main radar facies (RFsbf, RFsd, RFld) identified along the GPR line 79.

collapse balance to yield constant interglacial global mean sea level. We used this ensemble to find that because of GIA, simultaneous early MIS-5e Laurentide persistence and West Antarctic collapse can cause Apalachicola RSL to rise by 20+ mm/yr (early MIS-5e), then fall by up to −2 mm/yr, then rise by +2 mm/yr, then fall by 3–5+ mm/yr in late MIS-5e (Figure D). These magnitudes and tendencies are within the range of our RSL changes inferred from GPR. This suggests that the concurrent but asymmetric melt and regrowth of multiple ice sheets may be needed to explain the rapid RSL changes we observe.

The most probable candidate for rapid melt and regrowth is the West Antarctic Ice Sheet (WAIS), for two reasons. First, each 1 mm/yr of WAIS melt/regrowth would increase/decrease Apalachicola RSL by ~1.3 mm/yr due to the fingerprint of WAIS ice melt (Hay et al., 2014). Second, WAIS collapse in early MIS-5e, if it occurred, was likely triggered by ocean forcing (Clark et al., 2020). Once warm water incursion abated, low MIS-5e insolation during austral summer would have enabled some sectors of WAIS to regrow rapidly, as is suggested by the presence of the Ronne Ice Shelf by 126 ka (Wolff et al., 2025). The overlapping effects of WAIS regrowth, Laurentide Hudson Bay ice saddle collapse during the MIS-5e proglacial lake flooding event (Zhou and McManus, 2022), and concurrent Greenland melt (Yau et al., 2016), could have summed to magnitudes of RSL change similar to the changes we observed along the Apalachicola coast. This scenario would also better align the Apalachicola RSL rates with MIS-5e sea-level rates reported in the Red Sea (Rohling et al., 2019, Figure E), as the Red Sea WAIS fingerprint is ~75% that of Apalachicola (Hay et al., 2014).

5.3. *Other Late Pleistocene environmental records*

In addition to the RSL pattern, in the latter part of GPR Line 78, we identified seven erosional surfaces in Beach Ridge Set A that we interpret as erosion from storms (Fig. 6, Fig. 7C). From our age interpretations,

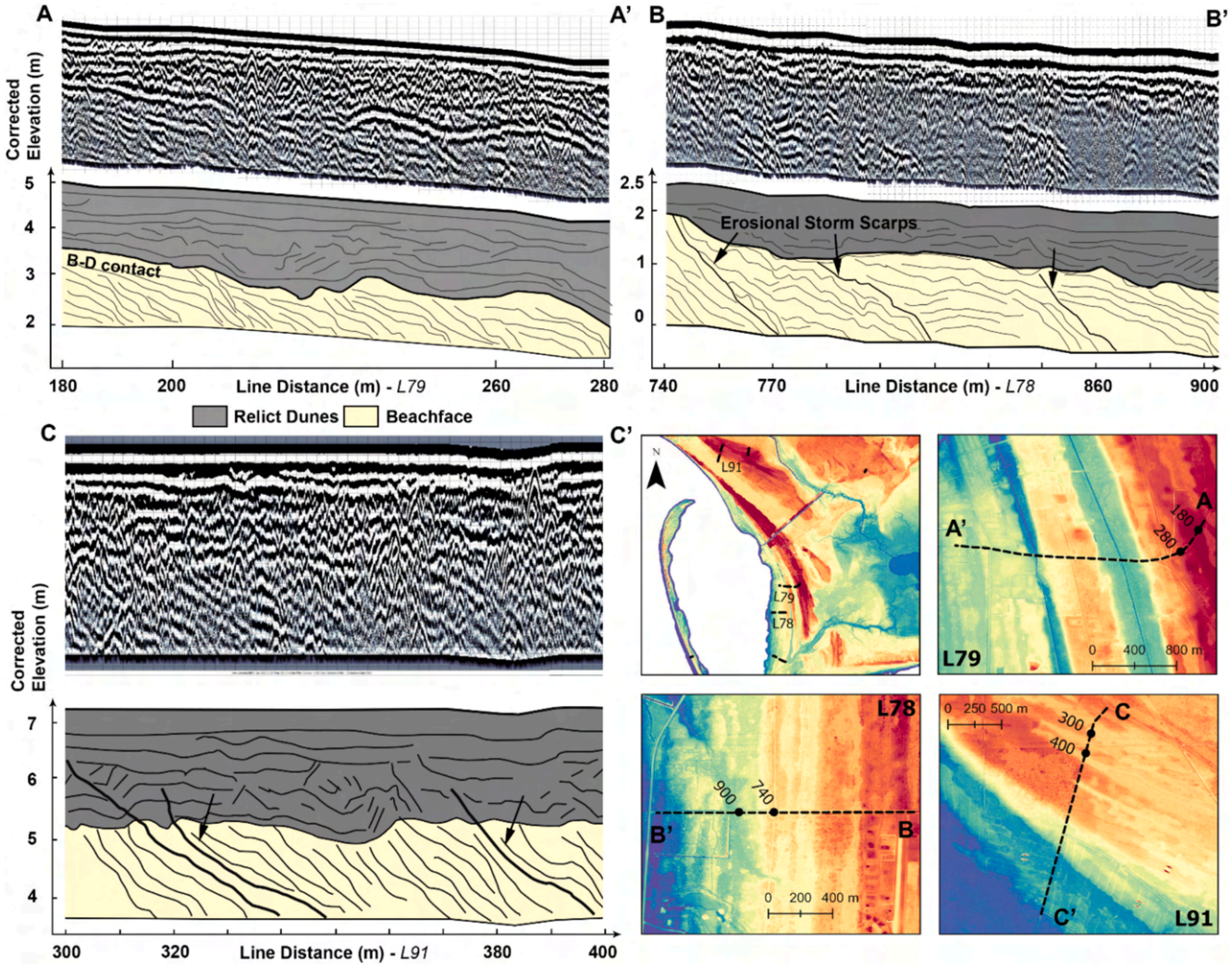

Fig. 6. Location of GPR profiles and interpretation for GPR lines L79, L78, and L91 (see full profiles and interpretation of radar surfaces in Supplementary Figs. 4,5 and 6). The profile locations are plotted on top of the 1-m resolution DEMs (US Geological Survey, 2022).

these seven erosional features were created during the very last part of MIS 5e (i.e., around 113–117 ka, Fig. 7E). Applying Holocene barrier progradation rates in this area, published by different authors (Forrest, 2007; Rink and López, 2010, 2015) and averaging only the long-term rates (>1 ka) obtained in this area (see Supplementary Table 1), we obtain that the long-term average barrier progradation rate in this area is 1.18 ± 0.11 m/yr.

Therefore, assuming a progradation rate equal to that during the Holocene, these seven storms happened over a period of ~540 years. This translates to a recurrence of one major storm every 76 years during late MIS 5e. This recurrence interval is lower than the historical record of hurricanes (one every 42 years, Rodysill et al., 2020), but higher than the estimated 12 extreme hurricanes over ~2500 years proposed for the Gulf of Mexico by Bregy et al. (2018). The greater frequency of storms during the historical record may suggest the GPR only captures events above a certain magnitude threshold (e.g., hurricane category ≥3), or that beach ridge formation is influenced primarily by such high-intensity events, whereas sediment cores may preserve a broader range of storm imprints.

5.4. *Paleogeographical evolution of the Apalachicola Barrier Island Complex*

Our results suggest that a coastal barrier system prograded during the early MIS5e highstand, forming a series of east-west oriented barrier islands and a north-south oriented strandplain attached at its west to older Pleistocene deposits (Fig. 8A). During the MIS5e RSL fall (Fig. 8B), the delta of the ancestral Apalachicola River prograded, eroding the strandplain and seabed near Cape San Blas and forming the channel now occupied by Depot Creek – which currently flows north but whose tributaries appear to indicate a southward directed flow at one time (Donoghue, 1993). After sea level rose during late MIS5e, the small river in Cape San Blas was bypassed and younger beach ridges nucleated from the Early MIS5e deposits (8C). Finally, during the Holocene transgression new smaller barrier islands formed south of the Pleistocene coastal barrier system. These islands, located along Cape San Blas, connected to the Pleistocene units as the Apalachicola River now rerouted to enter the Gulf east of its late MIS5e location (Fig. 8D).

6. Conclusions

We acquired new Ground Penetrating Radar (GPR) profiles and RTK measurements across modern and fossil beach ridges and strandplains in the Apalachicola River Delta area of northwest Florida. Combined with existing LiDAR-derived digital elevation models (DEMs) and Optically Stimulated Luminescence (OSL) ages, these data provide new insights into the region's response to sea-level changes over geological timescales. Based on this integrated analysis, we propose a coastal barrier

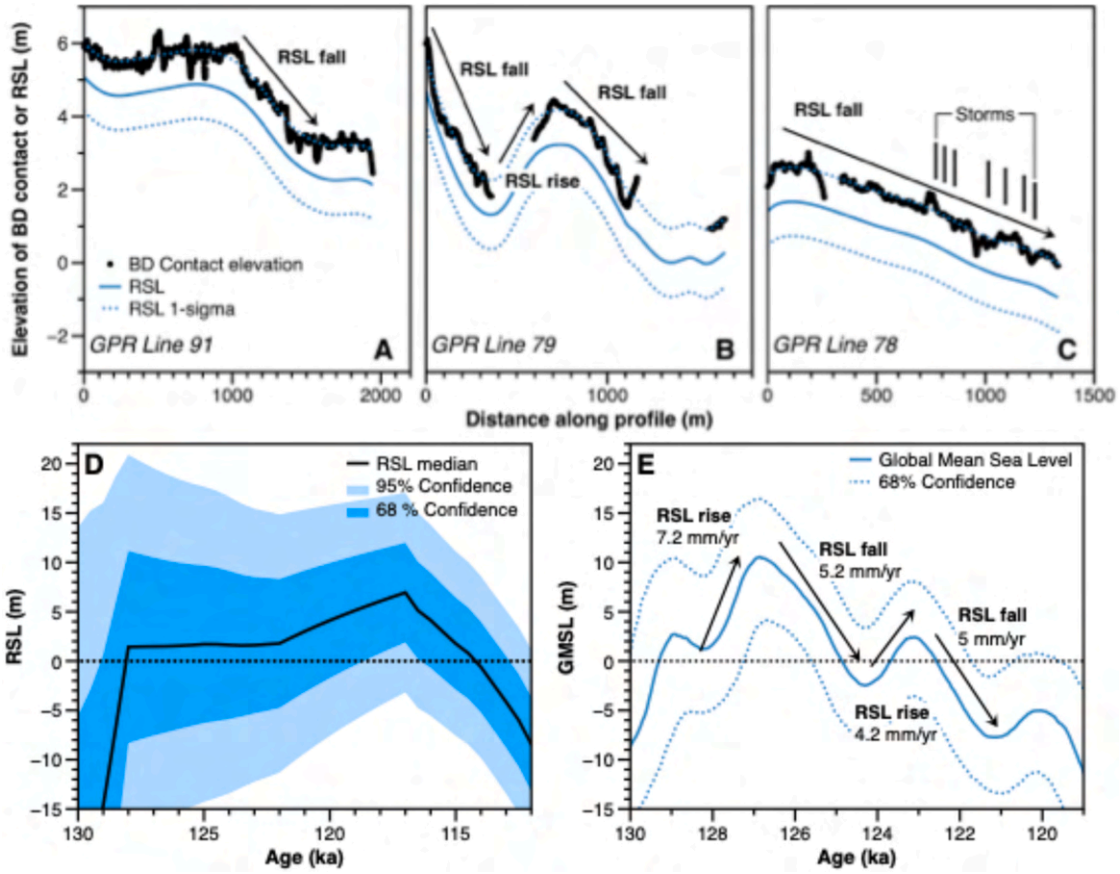

Fig. 7. A) Beach-Dune contact and associated RSL at GPR Line 91, interpreted as pre-MIS 5e (see text for discussion). B) and C) Same as A), but for GPR Lines 79 and 78, respectively representative of early / mid and late MIS 5e (see text for discussion). D) GIA relative sea level as predicted by glacial isostatic adjustment models at Cape San Blas (Creel and Austermann, 2025). E) GMSL during MIS 5e and associated rates as calculated by Rohling et al., 2019.

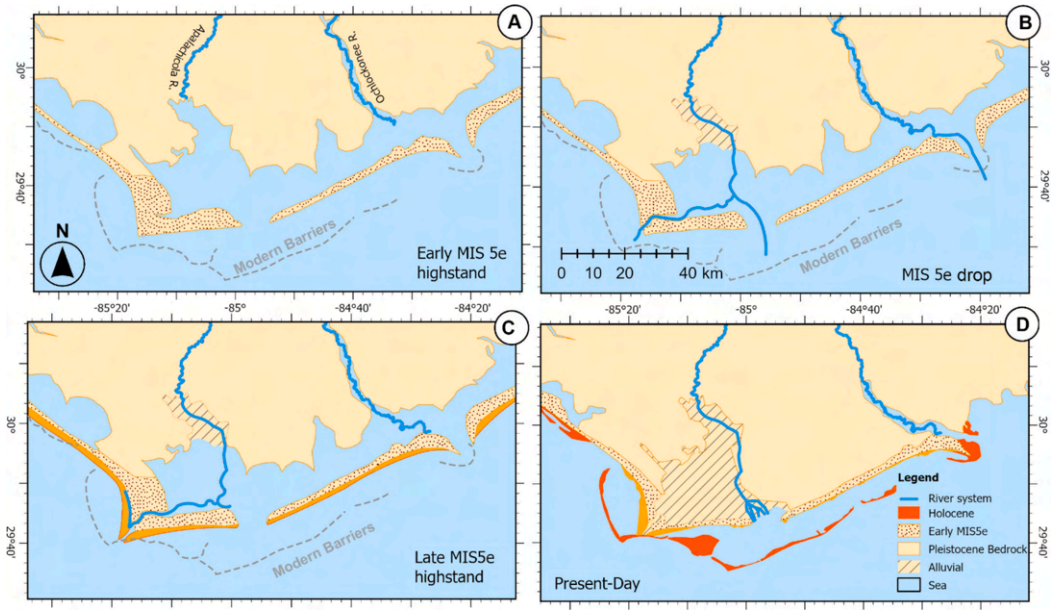

Fig. 8. Evolution of the Apalachicola coastal barrier system since the Last Interglacial (MIS5e). A) Early MIS 5e highstand; B). MIS5e drop, C) Late MIS5e highstand, D) Present-day coastal morphology.

evolution model for the broader Apalachicola Delta area from at least the Last Interglacial (MIS 5e) through the present. Our results suggest marine deposits extended across the Apalachicola Delta from elevations as high as +75 m (NAVD88) down to mean sea level, likely representing sedimentation from the Late Pliocene to Early Pleistocene. Coastal landforms such as spits, barriers, and sandbars are recognized, attesting

to the long and dynamic coastal history of the area.

Within the Pleistocene coastal sequences, the combination of GPR collected in this work, LiDAR, and OSL data from literature reveal the existence of three distinct beach ridge sets, the two most seaward of which we hypothesize were formed during the early and late phases of MIS 5e. These units appear to have been shaped by sea-level oscillations. While the age assignment of these two beach ridge sets relies on chronostratigraphic correlation with nearby cores, if the hypothesis that both sets were formed during the MIS 5e highstand is accepted, their separation might be linked to a sea-level fall associated with the regrowth of a collapsed West Antarctic Ice Sheet, coinciding with ongoing Laurentide and Greenland ice melt during MIS 5e. Further inland, we identified a third, stratigraphically older beach ridge plain, likely formed during a previous interglacial period (MIS 7, or older), although an early MIS 5e age cannot be excluded. The presence of MIS 6 alluvial deposits and better-preserved coastal sequences in the western delta supports the interpretation of a complex, multi-phase Pleistocene evolution. Additionally, erosional scarps identified in GPR profiles suggest the occurrence of major storm events approximately every 76 years during the latter part of MIS 5e, highlighting the dynamic interplay between storm activity and barrier development; however, this estimate is tentative, as it depends on assumptions about progradation rates, GPR resolution and the preservation of only higher-magnitude events.

CRediT authorship contribution statement

Nikos Georgiou: Writing – original draft, Methodology, Investigation, Conceptualization. **Alexander R. Simms:** Writing – original draft, Methodology, Investigation, Conceptualization. **Roger C. Creel:** Writing – review & editing, Methodology, Formal analysis. **Silas Dean:** Writing – review & editing, Investigation, Formal analysis. **Denovan Chauveau:** Writing – review & editing, Formal analysis, Data curation. **Ciro Cerrone:** Writing – review & editing, Investigation, Data curation. **Claudia Caporizzo:** Writing – review & editing, Formal analysis, Data curation. **Alessio Rovere:** Writing – original draft, Investigation, Funding acquisition, Conceptualization.

Declaration of competing interest

The authors declare the following financial interests/personal relationships which may be considered as potential competing interests: Alessio Rovere reports financial support was provided by Ca' Foscari University of Venice. If there are other authors, they declare that they have no known competing financial interests or personal relationships that could have appeared to influence the work reported in this paper.

Acknowledgements

This work was funded by the European Research Council (ERC) under the European Union's Horizon 2020 research and innovation programme (grant agreement n. 802414). The manuscript reflects only the view of the authors and the EU is not responsible for any use that may be made of the information it contains. RC was supported by a Woods Hole Oceanographic Institution Postdoctoral Scholarship.

Appendix A. Supplementary data

Supplementary data to this article can be found online at https://doi.org/10.1016/j.geomorph.2026.110404.

Data availability

Data is in Zenodo and there is a link in the MS

References

Barnett, R.L., Austermann, J., Dyer, B., Telfer, M.W., Barlow, N.L., Boulton, S.J., Carr, A. S., Creel, R.C., 2023. Constraining the contribution of the Antarctic Ice Sheet to Last Interglacial sea level. Sci. Adv. 9, eadf0198.
Boyd, R., Dalrymple, R., Zaitlin, B., 1992. Classification of clastic coastal depositional environments. Sediment. Geol. 80, 139–150.
Bregy, J.C., Wallace, D.J., Totten, R.L., Cruz, V.J., 2018. 2500-year paleotempestological record of intense storms for the northern Gulf of Mexico, United States. Mar. Geol. 396, 26–42. https://doi.org/10.1016/j.margeo.2017.09.009.
Brenneman, L., Tanner, W.F., 1958. Possible abandoned barrier islands in panhandle Florida. J. Sediment. Res. 28, 342–344.
Burdette, K.E., Rink, W.J., López, G.I., Mallinson, D.J., Parham, P.R., Reinhardt, E.G., 2012. Geological investigation and optical dating of Quaternary siliciclastic sediments near Apalachicola, North-west Florida, USA. Sedimentology 59, 1836–1849. https://doi.org/10.1111/j.1365-3091.2012.01328.x.
Butler, E.R.T., 1999. Process environments on modern and raised beaches in McMurdo Sound, Antarctica. Marine Geology 162 (1), 105–120. https://doi.org/10.1016/S0025-3227(99)00061-4.
Buynevich, I.V., FitzGerald, D.M., Goble, R.J., 2007. A 1500 yr record of North Atlantic storm activity based on optically dated relict beach scarps. Geology 35, 543–546.
Carruthers, E.A., Lane, D.P., Evans, R.L., Donnelly, J.P., Ashton, A.D., 2013. Quantifying overwash flux in barrier systems: An example from Martha's Vineyard, Massachusetts, USA. Mar. Geol. 343, 15–28.
Carter, R.W.G., 1986. The morphodynamics of beach-ridge formation: Magilligan, Northern Ireland. Marine Geology 73 (3–4), 191–214. https://doi.org/10.1016/0025-3227(86)90015-0.
Carvalho, R.C., Oliver, T.S.N., Woodroffe, C.D., 2019. Transition from marine to fluvial-dominated sediment supply at Shoalhaven prograded barrier, southeastern Australia. Geomorphology 341, 65–78. https://doi.org/10.1016/j.geomorph.2019.05.010.
Clark, P.U., He, F., Golledge, N.R., Mitrovica, J.X., Dutton, A., Hoffman, J.S., Dendy, S., 2020. Oceanic forcing of penultimate deglacial and last interglacial sea-level rise. Nature 577, 660–664.
Costas, S., Ferreira, Ó., Plomaritis, T.A., Leorri, E., 2016. Coastal barrier stratigraphy for Holocene high-resolution sea-level reconstruction. Sci. Rep. 6, 38726. https://doi.org/10.1038/srep38726.
Creel, R.C., Austermann, J., 2025. Glacial isostatic adjustment driven by asymmetric ice sheet melt during the Last Interglacial causes multiple local sea-level peaks. Geology 53, 253–258. https://doi.org/10.1130/G52483.1.
Creel, R.C., Kopp, R.E., Dutton, A., Zhou, Y., Raymo, M.E., Britt, C.J., DeConto, R.M., 2026. North American ice sheet persistence into past interglacials should inform future projections. Nat. Commun. https://doi.org/10.1038/s41467-026-70032-y.
Donnelly, C., Kraus, N., Larson, M., 2006. State of knowledge on measurement and modeling of coastal overwash. J. Coast. Res. 22, 965–991.
Donoghue, J.F., 1993. Late Wisconsinan and Holocene depositional history, northeastern Gulf of Mexico. Mar. Geol. 112, 185–205.
Donoghue, J.F., Stapor, F.W., Tanner, W.F., 1998. Discussion of: Otvos, EG, 1995. Multiple Pliocene-Quaternary Marine Highstands, Northeast Gulf Coastal Plain-Fallacies and Facts. Journal of Coastal Research, 11, 984–1002. J. Coast. Res. 669–674.
Dougherty, A.J., 2018. Prograded coastal barriers provide paleoenvironmental records of storms and sea level during late Quaternary highstands. J. Quat. Sci. 33, 501–517.
Dyer, B., Austermann, J., D'Andrea, W.J., Creel, R.C., Sandstrom, M.R., Cashman, M., Rovere, A., Raymo, M.E., 2021. Sea-level trends across the Bahamas constrain peak last interglacial ice melt. Proc. Natl. Acad. Sci. USA 118, 1–11. https://doi.org/10.1073/pnas.2026839118.
Fairbridge, R.W., Hillaire-Marcel, C., 1977. An 8,000-yr palaeoclimatic record of the 'Double-Hale'45-yr solar cycle. Nature 268, 413–416.
Farrell, W., Clark, J.A., 1976. On postglacial sea level. Geophys. J. Int. 46, 647–667.
Flemming, B., 1982. Xi. Beach morphodynamics in relationship to wave energy, grain size and internal sedimentary structure. Jt. Geol. Surv. Cape Town 97.
Forrest, B.M., 2007. Evolution of the beach ridge strandplain on st. Vincent island, florida (Ph.D. Thesis). The Florida State University.
Gernant, C., Simms, A.R., DeWitt, R., Theilen, B., Garcia, C.N., Goebel, M., 2025. Insights into the sea-level history of the South Shetland Islands from ground penetrating radar on Livingston Island, Antarctica. Quat. Sci. Rev. 359, 109363.
Goetschius, D.W., 1971. Preliminary Sedimentological and Geomorphological Study of Certain High Terrace Sands Between the Ochlockonee and Apalachicola rivers, Liberty and Gadsden Counties, Florida (PhD Thesis). Florida State University.
Golledge, N.R., Clark, P.U., He, F., Dutton, A., Turney, C.S.M., Fogwill, C.J., Naish, T.R., Levy, R.H., McKay, R.M., Lowry, D.P., Bertler, N.A.N., Dunbar, G.B., Carlson, A.E., 2021. Retreat of the Antarctic ice sheet during the Last interglaciation and implications for future change. Geophys. Res. Lett. 48, e2021GL094513. https://doi.org/10.1029/2021GL094513.
Goodwin, I.D., Mortlock, T.R., Ribo, M., Mitrovica, J.X., O'Leary, M., Williams, R., 2023. Robbins Island: The index site for regional Last Interglacial sea level, wave climate and the subtropical ridge around Bass Strait, Australia. Quat. Sci. Rev. 305, 107996.
Goslin, J., Clemmensen, L.B., 2017. Proxy records of Holocene storm events in coastal barrier systems: Storm-wave induced markers. Quat. Sci. Rev. 174, 80–119. https://doi.org/10.1016/j.quascirev.2017.08.026.
Hay, C., Mitrovica, J.X., Gomez, N., Creveling, J.R., Austermann, J., Kopp, R.E., 2014. The sea-level fingerprints of ice-sheet collapse during interglacial periods. Quat. Sci. Rev. 87, 60–69.
Hede, M.U., Bendixen, M., Clemmensen, L.B., Kroon, A., Nielsen, L., 2013. Joint interpretation of beach-ridge architecture and coastal topography show the validity

of sea-level markers observed in ground-penetrating radar data. The Holocene 23, 1238–1246.
Hein, C.J., Ashton, A.D., 2020. Long-term shoreline morphodynamics: processes and preservation of environmental signals. In: Sandy Beach Morphodynamics, pp. 487–531.
Hesp, P.A., 1984. Foredune formation in southeast Australia. In: Coastal Geomorphology in Australia. Academic Press, pp. 69–97.
Holdahl, S.R., Morrison, N.L., 1974. Regional investigations of vertical crustal movements in the US, using precise relevelings and mareograph data. Tectonophysics 23, 373–390.
Iizuka, M., Seki, O., Wilson, D.J., Suganuma, Y., Horikawa, K., van de Flierdt, T., Ikehara, M., Itaki, T., Irino, T., Yamamoto, M., Hirabayashi, M., Matsuzaki, H., Sugisaki, S., 2023. Multiple episodes of ice loss from the Wilkes Subglacial Basin during the Last Interglacial. Nat. Commun. 14, 2129. https://doi.org/10.1038/s41467-023-37325-y.
Isla, M.F., Moyano-Paz, D., FitzGerald, D.M., Simontacchi, L., Veiga, G.D., 2023. Contrasting beach-ridge systems in different types of coastal settings. Earth Surf. Process. Landf. 48, 47–71.
Jol, H.M., Smith, D.G., Meyers, R.A., 1996. Digital ground penetrating radar (GPR): a new geophysical tool for coastal barrier research (examples from the Atlantic, Gulf and Pacific Coasts, USA). J. Coast. Res. 960–968.
Komar, P.D., Wang, C., 1984. Processes of selective grain transport and the formation of placers on beaches. J. Geol. 92, 637–655.
Kopp, R.E., Simons, F.J., Mitrovica, J.X., Maloof, A.C., Oppenheimer, M., 2009. Probabilistic assessment of sea level during the last interglacial stage. Nature 462, 863–867. https://doi.org/10.1038/nature08686.
Kopp, R.E., Simons, F.J., Mitrovica, J.X., Maloof, A.C., Oppenheimer, M., 2013. A probabilistic assessment of sea level variations within the last interglacial stage. Geophys. J. Int. 193, 711–716. https://doi.org/10.1093/gji/ggt029.
Kuchar, J., Milne, G., Wolstencroft, M., Love, R., Tarasov, L., Hijma, M., 2018. The influence of sediment isostatic adjustment on sea level change and land motion along the U.S. Gulf Coast. J. Geophys. Res. Solid Earth 123, 780–796. https://doi.org/10.1002/2017JB014695.
Kumar, R., Switzer, A.D., Gouramanis, C., Bristow, C.S., Shaw, T.A., Jankaew, K., Li, T., Brill, D., 2024. Late-Holocene sea-level markers preserved in a beach ridge system on Phra Thong Island, Thailand. Geomorphology 465, 109405.
Lau, S.C.Y., Wilson, N.G., Golledge, N.R., Naish, T.R., Watts, P.C., Silva, C.N.S., Cooke, I. R., Allcock, A.L., Mark, F.C., Linse, K., Strugnell, J.M., 2023. Genomic evidence for West Antarctic Ice Sheet collapse during the Last Interglacial. Science 382, 1384–1389. https://doi.org/10.1126/science.ade0664.
Lindhorst, S., Schutter, I., 2014. Polar gravel beach-ridge systems: Sedimentary architecture, genesis, and implications for climate reconstructions (South Shetland Islands / Western Antarctic Peninsula). Geomorphology 221, 187–203. https://doi.org/10.1016/j.geomorph.2014.06.013.
Lopes, R.P., Pereira, J.C., Caron, F., Dillenburg, S.R., Rosa, M.L.C.D.C., Barboza, E.G., Savian, J.F., Sawakuchi, A.O., Tatumi, S.H., Yee, M., 2024. Stratigraphy and evolution of the late Pleistocene (MIS 5) coastal Barrier III in southern Brazil. Quat. Res. 1–23. https://doi.org/10.1017/qua.2023.67.
Masselink, G., van Heteren, S., 2014. Response of wave-dominated and mixed-energy barriers to storms. Mar. Geol. 352, 321–347.
Masselink, G., Kroon, A., Davidson-Arnott, R.G.D., 2006. Morphodynamics of intertidal bars in wave-dominated coastal settings — a review. Geomorphology 73, 33–49. https://doi.org/10.1016/j.geomorph.2005.06.007.
Mauz, B., Hijma, M., Amorosi, A., Porat, N., Galili, E., Bloemendal, J., 2013. Aeolian beach ridges and their significance for climate and sea level: concept and insight from the Levant coast (East Mediterranean). Earth-Sci. Rev. 121, 31–54.
Maxwell, R., 1971a. Preliminary ionium date from marine terrace, Florida. Coast. Res. Notes 3, 9–10.
Maxwell, R., 1971b. Origin and Chronology of Alabama River Terraces. GCAGS Trans.
Montes, A., Bujalesky, G.G., Paredes, J.M., 2018. Geomorphology and internal architecture of Holocene sandy-gravel beach ridge plain and barrier spits at Río Chico area, Tierra del Fuego, Argentina. J. South Am. Earth Sci. 84, 172–183.
Murray-Wallace, C.V., 2018. Quaternary History of the Coorong Coastal Plain, Southern Australia: An Archive of Environmental and Global Sea-Level Changes. Springer International Publishing, Cham. https://doi.org/10.1007/978-3-319-89342-6.
Nielsen, L., Bendixen, M., Kroon, A., Hede, M.U., Clemmensen, L.B., Weβling, R., Elberling, B., 2017. Sea-level proxies in Holocene raised beach ridge deposits (Greenland) revealed by ground-penetrating radar. Sci. Rep. 7, 46460.
Nienhuis, J.H., Ashton, A.D., Giosan, L., 2016. Littoral steering of deltaic channels. Earth Planet. Sci. Lett. 453, 204–214. https://doi.org/10.1016/j.epsl.2016.08.018.
NOAA National Centers for Environmental Information, 2023. Coastal Relief Models. NOAA National Centers for Environmental Information. https://doi.org/10.25921/5ZN5-KN44.
Nooren, K., Hoek, W.Z., Winkels, T., Huizinga, A., Van Der Plicht, H., Van Dam, R.L., Van Heteren, S., Van Bergen, M.J., Prins, M.A., Reimann, T., Wallinga, J., Cohen, K.M., Minderhoud, P., Middelkoop, H., 2017. The Usumacinta–Grijalva beach-ridge plain in southern Mexico: a high-resolution archive of river discharge and precipitation. Earth Surf. Dyn. 5, 529–556. https://doi.org/10.5194/esurf-5-529-2017.
Okazaki, H., Nara, M., Nakazato, H., Furusawa, A., Ito, K., Tamura, T., 2022. Coastal progradation associated with sea-level oscillations in the later phase of the Last Interglacial period, central Japan. Quat. Sci. Rev. 285, 107507.
Olariu, C., Bhattacharya, J.P., 2006. Terminal distributary channels and delta front architecture of river-dominated delta systems. J. Sediment. Res. 76, 212–233.
Oliver, T.S.N., Kennedy, D.M., Tamura, T., Murray-Wallace, C.V., Konlechner, T.M., Augustinus, P.C., Woodroffe, C.D., 2018. Interglacial-glacial climatic signatures preserved in a regressive coastal barrier, southeastern Australia. Palaeogeogr. Palaeoclimatol. Palaeoecol. 501, 124–135. https://doi.org/10.1016/j.palaeo.2018.04.011.
Otvos, E.G., 1992. Quaternary Evolution of the Apalachicola Coast, Northeastern Gulf of Mexico.
Otvos, E.G., 1995. Multiple pliocene-quaternary marine highstands, northeast Gulf Coastal plain: fallacies and facts. J. Coast. Res. 984–1002.
Otvos, E.G., 2000. Beach ridges — definitions and significance. Geomorphology 32, 83–108. https://doi.org/10.1016/S0169-555X(99)00075-6.
Phillips, M., Blenkinsopp, C., Splinter, K., Harley, M., Turner, I., 2019. Modes of berm and beachface recovery following storm reset: Observations using a continuously scanning lidar. J. Geophys. Res. Earth Surf. 124, 720–736.
Pico, T., 2020. Towards assessing the influence of sediment loading on Last Interglacial sea level. Geophys. J. Int. 220, 384–392. https://doi.org/10.1093/gji/ggz447.
Raymo, M.E., Lisiecki, L.E., Nisancioglu, K.H., 2006. Plio-Pleistocene ice volume, antarctic climate, and the global δ18O record. Science 313, 492–495. https://doi.org/10.1126/science.1123296.
Rink, W.J., López, G.I., 2010. OSL-based lateral progradation and aeolian sediment accumulation rates for the Apalachicola Barrier Island Complex, North Gulf of Mexico, Florida. Geomorphology 123, 330–342. https://doi.org/10.1016/j.geomorph.2010.08.001.
Rink, W.J., López, G.I., 2015. Corrigendum to "OSL-based lateral progradation and aeolian sediment accumulation rates for the Apalachicola Barrier Island Complex, North Gulf of Mexico, Florida" [Geomorphology 123 (2010) 330–342]. Geomorphology 241, 41. https://doi.org/10.1016/j.geomorph.2015.02.016.
Rodriguez, A.B., Meyer, C.T., 2006. Sea-level variation during the Holocene deduced from the morphologic and stratigraphic evolution of Morgan Peninsula, Alabama, USA. J. Sediment. Res. 76, 257–269.
Rodysill, J.R., Donnelly, J.P., Sullivan, R., Lane, P.D., Toomey, M., Woodruff, J.D., Hawkes, A.D., MacDonald, D., d'Entremont, N., McKeon, K., Wallace, E., Van Hengstum, P.J., 2020. Historically unprecedented Northern Gulf of Mexico hurricane activity from 650 to 1250 CE. Sci. Rep. 10, 19092. https://doi.org/10.1038/s41598-020-75874-0.
Rohling, E.J., Hibbert, F.D., Grant, K.M., Galaasen, E.V., Irvalı, N., Kleiven, H.F., Marino, G., Ninnemann, U., Roberts, A.P., Rosenthal, Y., Schulz, H., Williams, F.H., Yu, J., 2019. Asynchronous Antarctic and Greenland ice-volume contributions to the last interglacial sea-level highstand. Nat. Commun. 10, 5040. https://doi.org/10.1038/s41467-019-12874-3.
Ruz, M.-H., Allard, M., 1994. Coastal dune development in cold-climate environments. Phys. Geogr. 15, 372–380.
Scheffers, A., Engel, M., Scheffers, S., Squire, P., Kelletat, D., 2012. Beach ridge systems–archives for Holocene coastal events? Prog. Phys. Geogr. 36, 5–37.
Schnable, J.E., Goodell, H.G., 1968. Pleistocene-Recent Stratigraphy, Evolution, and Development of the Apalachicola Coast. Geological Society of America, Florida.
Scott, T.M., Campbell, K.M., Rupert, F.R., Arthur, J.D., Missimer, T.M., Lloyd, J.M., Yon, J.W., Duncan, J.G., 2001. Geologic Map of the State of Florida. Florida Geological Survey Tallahassee, Fla.
Shennan, I., 1986. Flandrian sea-level changes in the Fenland. II: Tendencies of sea-level movement, altitudinal changes, and local and regional factors. J. Quat. Sci. 1, 155–179. https://doi.org/10.1002/jqs.3390010205.
Shennan, I., Long, A.J., Horton, B.P., 2015. Handbook of Sea-level Research. John Wiley & Sons.
Simms, A.R., Anderson, John B., DeWitt, R., Lambeck, K., Purcell, A., 2013. Quantifying rates of coastal subsidence since the last interglacial and the role of sediment loading. Glob. Planet. Chang. 111, 296–308. https://doi.org/10.1016/j.gloplacha.2013.10.002.
Stapor Jr., F.W., Mathews, T.D., Lindfors-Kearns, F.E., 1991. Barrier-island progradation and Holocene sea-level history in southwest Florida. J. Coast. Res. 815–838.
Stattegger, K., Tjallingii, R., Saito, Y., Michelli, M., Thanh, N.T., Wetzel, A., 2013. Mid to late Holocene sea-level reconstruction of Southeast Vietnam using beachrock and beach-ridge deposits. Glob. Planet. Chang. 110, 214–222.
Tamura, T., 2012. Beach ridges and prograded beach deposits as palaeoenvironment records. Earth-Sci. Rev. 114, 279–297. https://doi.org/10.1016/j.earscirev.2012.06.004.
Tamura, T., Nanayama, F., Saito, Y., Murakami, F., Nakashima, R., Watanabe, K., 2007. Intra-shoreface erosion in response to rapid sea-level fall: depositional record of a tectonically uplifted strand plain, Pacific coast of Japan. Sedimentology 54, 1149–1162.
Taylor, M., Stone, G.W., 1996. Beach-ridges: a review. J. Coast. Res. 12.
US Geological Survey, 2011. National Elevation Dataset, 1/9 Arc-second.
US Geological Survey, 2022. 1-Meter Digital Elevation Model.
Wolff, E.W., Mulvaney, R., Grieman, M.M., Hoffmann, H.M., Humby, J., Nehrbass-Ahles, C., Rhodes, R.H., Rowell, I.F., Sime, L.C., Fischer, H., Stocker, T.F., Landais, A., Parrenin, F., Steig, E.J., Dütsch, M., Golledge, N.R., 2025. The Ronne Ice Shelf survived the last interglacial. Nature 638, 133–137. https://doi.org/10.1038/s41586-024-08394-w.
Yau, A.M., Bender, M.L., Robinson, A., Brook, E.J., 2016. Reconstructing the last interglacial at Summit, Greenland: Insights from GISP2. Proc. Natl. Acad. Sci. 113, 9710–9715. https://doi.org/10.1073/pnas.1524766113.
Zhou, Y., McManus, J., 2022. Extensive evidence for a last interglacial Laurentide outburst (LILO) event. Geology 50, 934–938. https://doi.org/10.1130/G49956.1.
Zurbuchen, J., Simms, A.R., Warrick, J.A., Miller, I.M., Ritchie, A., 2020. A model for the growth and development of wave-dominated deltas fed by small mountainous rivers: Insights from the Elwha River delta, Washington. Sedimentology 67, 2310–2331.